Influence of macrobenthos (*Meretrix meretrix Linnaeus*) on erosion-accretion processes in intertidal flats: A case study from a cultivation zone

Benwei Shi [a, b, c], Paula D. Pratolongo [d], Yongfen Du [e], Jiasheng Li [f], S L Yang [a*], Jihua Wu [g],

Kehui Xu [h,i], Ya Ping Wang [a] *

[a] *State Key Laboratory of Estuarine and Coastal Research, East China Normal University, Shanghai 200062, China.*
[b] *State Key Laboratory of Marine Geology, Tongji University, Shanghai 200092, China.*
[c] *Shanghai Key Lab for Urban Ecological Processes and Eco-Restoration, School of Ecological and Environmental Sciences, East China Normal University, 200241 Shanghai, China*
[d] *CONICET – Instituto Argentino de Oceanografía, CC 804, B8000FWB Bahía Blanca, Argentina.*
[e] *College of Marine Science and Engineering, Nanjing Normal University, Nanjing, Jiangsu 210023, China*
[f] *Ministry of Education Key Laboratory for Coast and Island Development, Nanjing University, Nanjing 210093, China.*
[g] *Ministry of Education Key Laboratory for Biodiversity Science and Ecological Engineering, Institute of Biodiversity Science, Fudan University, Shanghai 200433, China*
[h] *Department of Oceanography and Coastal Sciences, Louisiana State University, Baton Rouge, LA, 70803, USA.*
[i] *Coastal Studies Institute, Louisiana State University, Baton Rouge, LA, 70803, USA.*

Corresponding author information,

Telephone: 086-021-54836447;

Fax: 086-021-54836458;

Email address: slyang@sklec.ecnu.edu.cn（S L. Yang）

ypwang@sklec.ecnu.edu.cn (Y P. Wang).

Authors information,

Email address: bwshi@sklec.ecnu.edu.cn（Benwei Shi）;

paulapra@criba.edu.ar (Paula D. Pratolongo);

duyongfen@nju.edu.cn (Yongfen Du)

jihuawu@fudan.edu.cn (Jihua Wu)

kxu@lsu.edu(Kehui Xu).

lijiasheng1984@126.com (jiasheng Li)

Abstract The activity of benthic organisms can strongly influence sediment dynamics in an intertidal flat. However, few studies have conducted a quantitative assessments of the effect of benthic organisms on erosion-accretion processes under field conditions. The aim of this study was to quantify the effects of the benthic clam *Meretrix meretrix* Linnaeus on bed erodibility and sediment erosion-accretion processes in an intertidal flat. Within the cultivation zone at site A, *M. meretrix* is present in large numbers (up to 137 individuals/m^2). On the other hand, site B is located outside the cultivation zone. At this site, which is only 500 m away from site A alongshore, *M. meretrix* forms a sparse population with only 3.7 individuals/m^2. The results showed that the critical shear stress for erosion, denoted by τ_{ce}, was 0.22 and 0.32 N/m^2 at sites B and A, respectively, and the magnitudes of bed-level change were significantly higher at site A than site B. These results reveal the large effect of *M. meretrix* on decreasing τ_{ce}, augmenting the erosion rate when the bed shear stress due to combined currents and waves, denoted by τ_{cw}, was higher than τ_{ce}, and conversely enhancing the accretion rate when $\tau_{cw} < \tau_{ce}$. The changes induced in these parameters are likely to have a large impact on model predictions of bed erodibility, sedimentary processes, and morphological evolution. Thus, integrated field measurements of hydrodynamic and bed-level changes, accompanied by simultaneous biological sampling, may help to improve the parameterization of hydro-sedimentary and morphodynamic models for shallow-water environments.

Plain Language Summary

The marine organisms in the bottom sediments can play an important role in the stability and erosion-accretion of the seafloor in the near-shore coastal area. However, less is known about how these organisms affect bed stability and erosion-accretion processes in shallow-water environments. This study uses integrated field measurements of hydrodynamics, erosion-accretion events and simultaneous biological sampling to quantify the effects of benthic organisms on seafloor stability and erosion-accretion processes. The results suggest that the

stability of the seafloor at the observation site with plenty of clam *Meretrix meretrix* Linnaeus is less stable, and the magnitude of seafloor erosion-accretion is greater compared to the observation site without clam *Meretrix meretrix*. These results have important implications for improving the parameterization of predicted models of morphological evolution due to the major biological components in estuaries and coastal regions.

Keywords: Benthic organism; Bed erodibility; Bed shear stress; Sedimentary process; Bed-level change.

1. Introduction

Intertidal flats are major components of estuaries and protected shorelines that are submerged at high tide and exposed at low tide. Intertidal flats are habitats of ecological significance (e.g., Mouritsen and Poulin, 2002; Gao, 2009; Adam et al., 2011) and generally support many types of marine animals such as *crabs*, *mollusks*, *flatfish* and turtles (e.g., Dyer, 2000; Barbier, 2013; Li et al., 2018), which provides rich feeding grounds for migratory shorebirds (e.g., Nehls and Tiedemann, 1993; Eisma, 1998; Adam et al., 2011). In addition, intertidal flats play an important role in coastal defense by helping to dissipate wave energy (Chen and Zong, 1998; Kirby, 2000; Möller et al., 2001; Bale et al., 2006). Morphodynamic models are widely used for the sustainable management of fisheries and aquaculture, coastal planning, habitat conservation, restoration of intertidal ecosystems, and mitigation of coastal hazards (Resio and Westerink, 2008; Dietrich et al., 2011; Wu et al., 2018). The interactions among biological and physical processes are known to modify the hydrology and sediment dynamics in the intertidal zone, which greatly affects morphodynamics (Tolhurst et al., 2000; Widdows and Brinsley, 2002; Grabowski et al., 2011; Wu et al., 2017). Thus, knowledge of the interplays among the physical forces and biological components of intertidal ecosystems is a critical step towards improving the parameterization of models of erosion-accretion processes and the morphological evolution of intertidal flats.

Previous studies have shown that benthic macrofauna can strongly influence sediment erodibility (e.g., Rhoads and Boyer, 1982; Bouma et al., 2001; Needham et al., 2013; Gao et al., 2014; Gerwing et al., 2016). Moreover, biological activity may influence the hydrodynamics of the bottom boundary layer by altering surface sediment roughness (e.g., O'Riordan et al., 1995; Jackson et al., 2007; Folmer et al., 2014; Harris et al., 2016). For example, benthic macrofauna can influence the nature and size distribution of bottom or suspended sediment particles through their feeding activities, which may involve the repackaging and biodeposition of suspended sediment particles and the formation of compact fecal pellets (Nowell et al., 1981; Wood and Armitage, 1997; Wotton and Malmqvist, 2001; Grabowski et al., 2011; McCall, 2013). The combined effects of living organisms may change the erosion-accretion rates by several orders of magnitude (Paterson and Black, 1999; Tolhurst et al., 2000).

Regarding the effects of benthic organisms on mudflat sediment erodibility, two different functional groups can be recognized. The behavior of some organisms enhances sediment biostabilization (e.g., benthic microalgae and some filter feeders; e.g., Luckenbach, 1986; Nasermoaddeli et al., 2014) by increasing the critical erosion threshold of bed sediment, thus reducing erosion rates (Nasermoaddeli et al., 2014). For example, mussels at high densities can protect the underlying sediment from erosion caused by waves and currents through an armoring effect (e.g., Widdows et al., 1998b, 2000). Similarly, mucus production by meiofauna and macrofauna organisms may contribute to sediment erodibility through the binding of sediment grains (e.g., de Brouwer et al., 2000; Grabowski et al., 2011). In contrast, the behavior of other organisms leads to biodestabilization, including several species of *crabs* and *mollusks* such as *Macoma balthica* and *Hydrobia ulvae* (e.g., Scoffin, 1970; Gage, 1977; Eckman et al., 1981; Harvey and Luoma, 1985; Tallqvist, et al., 2001; Meysman et al., 2006). The intense activity of these organisms (e.g., bioturbation) can reduce the critical erosion threshold and

eventually enhance erosion (Nasermoaddeli et al., 2014). However, in some cases, a single species can fulfill both roles. For example, *Corophium volutator* (*C. volutator*) can exacerbate erosion due to grazing on stabilizer diatoms and by reworking of bottom sediment during burrowing (Gerdol and Hughes, 1994); however, this same species is also able to increase the shear strength of bottom sediments by secretion of particle-binding substances, which has a stabilizing effect (Meadows and Tait, 1989; Mouritsen et al., 1998). Thus, a single species can have opposing effects on bed stabilization, and the overall effect on erosion thresholds and rates may depend on different environmental factors, such as the seasonal growth of benthic diatoms and faunal densities (Grant and Daborn, 1994).

Most studies that aim to improve our understanding of the interactions among benthic macrofauna, the physical properties of sediments, and hydrodynamic processes are based on well-controlled laboratory experiments (e.g., Eckman, 1983; Grant and Daborn, 1994; Orvain et al., 2004; Venier et al., 2012). In such studies, "intact" sediment samples are transported from the field to the laboratory for testing; however, it is difficult to obtain truly undisturbed sediment. Sediment samples are removed from a naturally dynamic environment. During excavation and transport, the physical properties of the sample (e.g., water content, consolidation, structure, and temperature) and ongoing benthic biological activity (e.g., burrowing by macrofauna and the production of extracellular polymeric substances by algae) are disturbed, leading to inaccurate quantifications. Field experiments using flumes and natural sediments containing macrofauna overcome some of these limitations, but flumes still disturb the natural flow fields (Widdows et al., 1998a; Widdows and Brinsley, 2002). To date, few *in situ* studies have sought to estimate the effects of benthic organisms on erosion-accretion processes under natural tidal current and wave conditions.

The aim of this study was to explore the effect of *Meretrix meretrix* Linnaeus (*M. meretrix*) on sediment erodibility and erosion-accretion processes under natural conditions. The results

from this study can be used for more accurate parametrization of morphodynamic and sediment transport models.

2. Study area

The study area is situated on the Rudong intertidal flat in the southeastern part of the Jiangsu Coast, China. The flat is located between the abandoned Yellow River Delta and the Yangtze River Estuary, adjacent to the largest radial-shaped tidal sand ridges on the Chinese continental shelf (Fig. 1A) (Wang et al., 2012; Xing et al., 2012). Typically, intertidal flats in this area span several tens of kilometers (e.g., Wang and Zhu, 1994; Shi et al., 2015). The Rudong intertidal flat is characterized by a high-energy hydrodynamic environment, with an average tidal range of 3.9-5.5 m, reaching a maximum of 7-8 m (Zhao and Gao, 2015). Spring tidal currents on the intertidal flat average 0.59 m/s, with higher current velocities during the ebb tide (Zhao and Gao, 2015). The maximum current velocity recorded on the lower intertidal flat was 1.22 m/s (Xing et al., 2012).

M. meretrix is an edible bivalve of the Mytilidae family and is characterized by a delicate taste, relatively high meat yield, and attractive appearance, making it an important commercial species (He et al., 1997). This bivalve is the main maricultural species along the Jiangsu Coast, with the largest cultivation zone in China located on the Rudong intertidal flat (e.g., Na, 2004; Shen, 2004; Li et al., 2014) owing to the favorable tidal flow and abundant nourishment provided by the radial tidal sand ridge system (Fig. 1B). In this study, site A is characterized by a high density of *M. meretrix*, given its location in the cultivation zone, whereas *M. meretrix* is not cultivated at site B and therefore is relatively rare (Fig. 1C, Fig. 2).

3. Methods

3.1 Field measurements of hydrodynamic data

Within each site, A and B, one observation site was established to measure hydrodynamic parameters. Field data were collected from August 24 to September 1, 2016 using a custom-

made frame with two stainless steel legs (Fig. 3), which were pushed at least 1.5 m into the sediment to maintain frame stability during data collection. All instruments were attached to this frame to collect time series of water depth, wave height, turbulent velocity in the near-bed boundary layer, and bed-level elevation.

A wave-tide recorder (SBE 26 Plus; Sea-Bird Electronics, USA) was mounted horizontally onto a frame, and its pressure sensor was located 0.1 m above the sea bed to measure water depth, wave height, and wave period (Fig. 3). The recorder used pressure sensors to collect data at a frequency of 4 Hz over a 256-second period, making 1024 measurements per 10 minutes (Table 1). Water depths were later corrected for the 0.1 m height difference between the recorder and sea bed (Fig. 3).

To investigate the turbulent velocity in the near-bed boundary layer, a Vector 6 MHz Acoustic Doppler Velocimeter (ADV; Nortek, USA) was used, which was mounted on the same frame in a vertical position 0.37 m above the sea bed (Fig. 3). Data were collected at 5-minute intervals with a frequency of 16 Hz (Table 1). The ADV recorded the distance to the bed surface at 1 Hz in an autonomous mode. Furthermore, information on erosion and accretion based on the time series of bed elevation was collected during a given phase. The accuracy of bed elevation measurements is ±1 mm and has already been investigated in the laboratory (Salehi and Strom, 2012) and in the field (Andersen et al., 2007). Thus, according to these studies, changes in bed elevation greater than 1 mm should be considered true bed-level changes during data collection.

In addition, hourly data on wind speeds and directions at the Rudong gauging station were obtained from the Yellow Sea Monitor Center, Weather Bureau of Jiangsu, China. In this study, the two regimes were divided based on the magnitude of wind speeds.

3.2 Field sampling of benthic organisms

Three sampling plots were randomly distributed around observation sites A and B and named A_1-A_3 and B_1-B_3, respectively, as shown in Fig. 1C. On 25 September 2016 at 11:00 (Beijing time), during aerial exposure of the study area (after ebb tide), three sediment samples with volumes of 0.3 m × 0.3 m × 0.1 m depth were taken from each sampling plot (18 samples in total) to estimate the abundance of benthic organisms. In the field, sediment samples from the same plot were mixed together and washed through a 1 mm mesh sieve, and all the residues were preserved in 10% formalin solution before further analysis.

Bottom sediment samples were collected at both sites close to the frame to calculate the grain-size distribution and water content. The grain-size distribution was measured using a laser particle size analyzer (Mastersizer 2000; Beckman Coulter, California, USA). For measurements of water content, wet sediment samples were immediately weighed and then oven-dried at 50°C until a constant weight was achieved (generally ≥ 48 h). Then, the percent water content was estimated as the ratio of the mass loss during drying to the sediment dry weight.

3.3 Data processing

3.3.1 Bed shear stress due to currents and waves

The bed shear stress generated by waves (τ_w, N/m^2) and currents (τ_c, N/m^2) was calculated according to A.2 and A.4 in Appendix A, respectively, and the bed shear stress due to combined currents and waves (τ_{cw}, N/m^2) was subsequently calculated using a current-wave hydrodynamic model (A.5 in the Appendix).

3.3.2 Critical shear stress for erosion (τ_{ce})

Following the approach recommended by Andersen et al. (2007) and Shi et al. (2015), we estimated the critical shear stress for erosion (τ_{ce}) at sites A and B, respectively, through comparisons between τ_{cw} and the corresponding change in bed level (erosion-accretion event).

The value of τ_{ce} was set as the value of τ_{cw} at which the erosion event had just begun.

3.3.3 Statistical comparisons

To investigate the differences between both sites regarding hydrodynamic conditions, factorial two-way ANOVA (Analysis of Variance) tests were performed considering the fixed effects of wind regime and site. Variables were wave heights, current velocities, and bed shear stresses due to combined currents (τ_{cw}) and waves, which were averaged over each tidal cycle. When necessary, data were log-transformed to meet the ANOVA assumptions of normality and homoscedasticity.

4. Results

4.1 Characterization of *M. meretrix* populations and bottom sediments

Within the cultivation area at site A, *M. meretrix* had an average density of 137 individuals per m^2 (range of 122-167) in the top 10 cm of the intertidal flat (Table 2). The average length, width, and height of *M. meretrix* were 31.0 mm (range of 30.8-31.7 mm), 25.7 mm (range of 24.8-26.9 mm), and 15.5 mm (range of 15.1-15.9 mm), respectively. The mean individual weight was 8.4 g (range of 7.8-8.9 g) at this site (Table 2).

Outside the cultivation area at site B, a single individual was found in one sample from site B$_3$ (Fig. 1C). Thus, the average density was 3.7 individuals per m^2 at this site. The only specimen found at site B (length, width, height, and weight of 40.3 mm, 34.1 mm, 20.6 mm, and 17.8 g, respectively) was much larger than the largest individual at site A (Table 2).

The median grain size at site B ranged from 135.8 to 144.7 μm (139.8±3.0 μm on average), compared with the range of 101.7 to 117.2 μm (111.6±5.2 μm on average) at site A. The water content was lower at site B (from 26.4% to 33.3%, 29.2±2.4% on average) than at site A (32.0% to 35.0%, 33.7±1.1% on average) (Fig. 4). Furthermore, from the grain-size distribution of the bed sediment, the proportion of coarse sediment at site B was higher than that at site A (Fig. 5), indicating that the presence of *M. meretrix* has changed the proportion of grain sizes in the

intertidal flat.

4.2 Wind, waves, currents and bed shear stress

During the entire field measurement, two wind regimes were distinguished from the time series of wind data based on the magnitude of wind speeds. Wind during tides T_1 to T_3 is characterized by mild winds (average and maximum wind speeds are 3.8 and 5.5 m/s, respectively) with southwest directions (Regime I, Beaufort numbers 0 to 3). Conversely, wind during tides T_4 to T_8 is characterized by stronger winds (average and maximum wind speeds are 8.6 and 12.7 m/s, respectively) with a dominant northwest directions (Regime II, Beaufort numbers > 3), compared with the wind during tides T_1 to T_3. Wind during tides T_9 to T_{11} is also a weak wind (average and maximum wind speeds are 3.2 and 5.2 m/s, respectively) with northeast directions (Regime I, Beaufort numbers 0 to 3) (Fig. 6a).

At both sites, wave heights were lower under the milder winds of Regime I (T_1-T_3 and T_9-T_{11}) and higher during T_4 to T_8 (Fig. 6b). At site A, wave heights ranged from ~0 to 2.0 m, with an average of 0.4 m during field measurement. At site B, despite the short distance between sites, higher values were found, ranging from ~0 to 2.6 m and 0.6 m on average (Fig. 6b).

During the entire field measurement, the lowest current velocities were recorded around high tides. Higher velocities characterized early flood and late ebb stages, and the average current velocities during flood tides were higher than those during ebb tides (Fig. 6c). A general counterclockwise rotation in the current direction was observed, with a southwestward (onshore) current during early flood tides, southeastward (alongshore) during high tides, and eastward or northeastward (offshore) during late ebb tides (Fig. 6d).

At both sites, tidal-averaged values of τ_w were higher during T_4-T_8 than during T_1-T_3 and T_9-T_{11} (Fig. 7b; Table 3). Tidal-averaged τ_{cw} values followed the same pattern, with lower values during T_1-T_3 and T_9-T_{11} (Table 3). Regarding τ_{cw}, similar values were observed between sites, ranging from ~0 to 0.73 N/m^2 at site A, compared with ~0 to 0.74 N/m^2 at site B (Fig.

7d).

4.3 Comparison of hydrodynamic conditions

During the entire field measurement, τ_{cw} during T_4-T_8 was higher than during T_1-T_3 and T_9-T_{11} (Table 3) due to the action of stronger wind during T_4-T_8. Thus, based on the strength of the hydrodynamic conditions, in this study, the three variables (wave heights, current velocities, and bed shear stresses due to combined currents and waves) averaged over the 11 tides were also grouped into two levels: Regime I (Tides T_1 to T_3 and T_9 to T_{11}) and Regime II (T_4 to T_8). The second factor was site, with two levels (within the cultivation area of site A and outside the cultivation area of site B).

Regarding wave heights (Fig. 8a), a significant interaction was observed between factors ($p < 0.01$), with higher waves at site B under the mild winds of Regime I (Tuckey post hoc comparisons, $p < 0.01$). Under stronger winds (Regime II), there were no significant differences in wave heights between sites ($p > 0.01$). Within sites, waves were significantly higher under wind Regime II. When current velocity and combined wave-current bed shear stress are considered, no significant interactions was observed between factors nor were there differences between sites ($p > 0.01$). Both sites responded similarly to wind regimes, with lower values for both variables under the mild conditions of Regime I ($p < 0.01$, Fig. 8b and c).

4.4 Erosion-accretion processes

At both sites, the time series of bed elevation did not show significant changes (>1 mm) during T_1-T_3, and erosion events began to occur only at the initial flooding stage of tide 4. During tide 4 at site A, the onset of erosion corresponded to a τ_{cw} value of 0.22 N/m^2 at the initial stage of flooding (Fig. 7d, 7e), while at site B, the onset of erosion corresponded to a τ_{cw} value of 0.32 N/m^2 during high tide (Fig. 7d, 7e). Therefore, these values (0.22 and 0.32 N/m^2) were considered to be the τ_{ce} values for sites A and B, respectively (see section 3.3.2).

At both sites, changes in bed-level during tides T_1-T_3 never exceeded the ±1 mm threshold for change detection, so neither erosion nor deposition events were identified (Fig. 7e; Table 3). Once τ_{ce} was reached at both sites, bed levels were progressively lower (erosion phase) during T_4-T_8 and progressively higher during T_9-T_{11} (accretion phase). Although sites A and B showed the same erosion-accretion trends for a given tide, the magnitude of change differed (Fig. 7e). During the erosion phase (tides T_4-T_8), the total bed-level change at site A was -97 mm (negative denotes erosion), whereas that at site B was -39 mm (Fig. 7e; Table 3). Similarly, the total bed-level change during the accretion phase (T_8-T_{11}) was +30 mm (positive denotes accretion) at site A and only +15 mm at site B (Fig. 7e; Table 3).

5. Discussion

The results showed that critical shear stress (i.e., erosion rate and bed erodibility) is lower at site A (0.22 N/m^2, with abundant *M. meretrix*) than at site B (0.32 N/m^2, without *M. meretrix*), suggesting that there is a link between critical bed shear stress (i.e., erosion rate) and the density of *M. meretrix*. This correlation is consistent with the results of previous field and laboratory studies. For example, on the Molenplaat tidal flat in Westerschelde (SW Netherlands), Widdows et al. (2000) reported that there was a positive relationship between sediment erosion rate and the density of the clam *Macoma balthica* (*M. balthica*), which is a major bioturbator of bottom sediments, and the tidal flat had a lower sediment erosion rate in June compared to September 1996 because the density of *M. balthica* is lower in June than in September 1996. Additionally, laboratory flume experiments have shown that bioturbation induced by *M. balthica* causes a density-dependent increase in sediment erodibility (Widdows et al., 1998b), and the destabilizing effects of this species have been demonstrated in modeling studies (Willows et al., 1998). In the previous studies mentioned above, changes in sediment erosion rate have been attributed to the enhanced grazing activity of deposit feeders such as *M. balthica*.

In this study, *M. meretrix* is a type of bivalve and has been known to show significant vertical movement, occasionally exposing their posterior shell edges before completely reburying themselves within a single day (Fig. 2). Thus, this activity of *M. meretrix* has been described as a major bioturbation (biological reworking of sediments) and has greatly influenced critical bed shear stress due to the activity of *M. balthica* mentioned above. The shallow-buried bivalves (e.g., *M. meretrix*) generally inhabit sandy substrate in lower intertidal and shallow subtidal areas, are buried to a depth of approximately 6 cm below the sediment surface (Zhuang and Wang, 2004), and tend to be mobile, resulting in greater bioturbation of the uppermost sediment layer. Considering the above analysis, this study can serve as a the reference for other bivalves that are widely distributed along coastlines worldwide, including China, Japan, Korea, India, and England (Navarro et al., 1991; Widdows et al., 2002; Liu et al., 2006).

The accretion rate was higher at site A under the effects of a large population of *M. meretrix* than at site B (Fig. 7), and the presence of bivalve *M. meretrix* could change the proportion of grain size (Fig. 5). This case is associated with the suspension-feeding behavior of *M. meretrix*, which is a siphonate clam that feeds on plankton and filters nutritious suspended particles in the tidal water through its incurrent siphon (Boehm and Quinn, 1976; Cohen et al., 1984; Carlton et al., 1990; Navarro et al., 2014; Burge et al., 2016; Yu et al., 2016). Specifically, the enhanced accretion and change in the proportion of sediment grain size at site A likely resulted from the feeding behavior of a large population of *M. meretrix*. This behavior may cause a localized increase in biodeposition and an associated increase in the downward flux of suspended material and promote biodeposition (Ward and Shumway, 2004), changing the proportion of sediment grain size due to the presence of *M. meretrix* at site A. The increased biodeposition by suspension-feeding bivalves is also supported by benthic annular flume experiments under both field and laboratory conditions. Widdows et al. (1998b) studied

biodeposition fluxes in mussel beds (dense populations of bivalve mollusk *Mytilus edulis*) in Cleethorpes, Humber Estuary, and found that deposition rates were linearly related to mussel density, up to a maximum of 60 g m^{-2} h^{-1} at densities of 1400 mussels per m^2 (corresponding to 50% mussel cover). Biodeposition at this density was an order of magnitude higher than physical deposition at 0% mussel cover. Additionally, during field measurements, potential disturbances from human activities are excluded at site A, i.e., the harvesting of *M. meretrix* is not an anthropogenic factor that affects erosion-accretion processes. The farmers harvested calm *M. meretrix* in the cultivation zone every two years, and the gap between harvesting and our field survey is approximately one and a half years. In summary, the difference in erosion-accretion processes is likely mainly due to the presence of *M. meretrix* rather than other potential factors.

The present analysis above revealed that the bivalve *M. meretrix*, at high densities, plays a significant role in sediment dynamics and bed erodibility. Thus, biologically driven changes in τ_{ce} and accretion rates need to be considered in morphodynamic and sediment transport models of shallow-water environments. However, the effects of *M. meretrix* are complex in natural environments, and parametrizations based on laboratory experiments can lead to large biases. We propose a multidisciplinary field measurement approach that combines hydrodynamic, sedimentary, and biological sampling to quantify and model the naturally occurring biological influence on sediment dynamics. Future work should be directed to improving field data acquisition by automatization and improving the temporal resolution (Collins et al., 1998). Biological sampling should be accompanied by the collection of current, wave, and bed-level data to better describe the key biological-physical interactions and the mechanisms involved. In addition, a more complete understanding is needed for the population dynamics of dominant benthic organisms, including benthic microalgae, infaunal deposit and filter feeders, and epibenthic organisms. Finally, field measurements of natural environments

should be compared with measurements from controlled experiments, including factors such as faunal exclosures, manipulated densities of benthic animals, and nutrient additions that may promote microalgae growth.

6. Conclusions

The results show that *M. meretrix* can significantly affect erosion-accretion processes on an intertidal flat of the Jiangsu Coast, China. Integrated measurements of waves, near-boundary turbulent velocities, and bed-level changes were collected under natural conditions. Measurements of physical parameters were combined with simultaneous estimations of *M. meretrix* density to quantify the effects of this species on sediment dynamic processes. The main conclusions are summarized as follows. First, the τ_{ce} values at site B, without *M. meretrix*, were ~1.5 times higher than those at site A, where *M. meretrix* is abundant (0.32 vs 0.22 N/m^2, respectively). This major difference in τ_{ce} (bed erodibility) between the sites is inferred to relate to *M. meretrix* bioturbation, as frequent vertical movements cause destabilization of seafloor sediment. Second, erosion processes were stronger at site A than site B. Simultaneous measurements of sediment properties suggest that the biological activity of *M. meretrix* at site A results in increased sediment water content, further enhancing the erosion rate under conditions of $\tau_{cw} > \tau_{ce}$. Third, accretion processes were greater at site A than site B. The presence of *M. meretrix,* a filter-feeding bivalve, resulted in an enhanced biodeposition flux at site A during the accretion phase ($\tau_{cw} < \tau_{ce}$). This higher deposition rate of suspended sediments at cultivated sites may have important implications for sediment transport. These conclusions allow for a more accurate parametrization of biological effects, thus helping to refine the numerical models of sediment transport and morphodynamics. These models are critical to environmental engineers and coastal managers who face the major challenge of predicting the impacts of construction projects in shallow estuarine and coastal environments with extensive intertidal areas and high abundances of benthic organisms.

Appendix A: Estimation of bed shear stress

The wave orbital velocity ($\widehat{U}_\delta$) at the edge of the wave boundary layer can be expressed as follows:

$$\widehat{U}_\delta = \frac{\pi H}{T \sinh\left(\frac{2\pi}{L} h\right)} \tag{A1}$$

where L [$= (gT^2/2\pi) \tanh(2\pi h/L)$] is wavelength (m), g is acceleration due to gravity (= 9.8 m/s^2), H is wave height (m), T is wave period (s), and h is water depth (m).

The bed shear stress due to waves (τ_w) is related to $\widehat{U}_\delta$ and the wave friction factor (f_{wr}), which is as follows:

$$\tau_w = 0.5 \, \rho_w f_{wr} \, \widehat{U}_\delta{}^2 \tag{A2}$$

where ρ_w is the density of seawater (=1030 kg/m^3). According to Soulsby (1997), f_{wr} under fully turbulent regimes can be estimated as follows:

$$f_{wr} = 0.237 \, r^{-0.52} \tag{A3}$$

where r ($= \hat{A}_\delta / k_s$) is the relative roughness, $\hat{A}_\delta$ ($= \widehat{U}_\delta T / 2\pi$) is the semiorbital excursion, k_s (=2.5 d_{50}) is the Nikuradse equivalent sand grain roughness, d_{50} is the median grain size of bottom sediments, and $\widehat{U}_\delta$ is the wave orbital velocity (Equation A1).

Turbulent velocities from ADV records can be decomposed into mean and fluctuating components (i.e., $\mathbf{u} = \bar{\mathbf{u}} + \mathbf{u}'$, where u is the measured velocity, $\bar{\mathbf{u}}$ is the mean velocity, and u$'$ is the mean turbulent velocity), as well as horizontal and vertical components. The bed shear stress due to current (τ_c, N/m^2) can be estimated from fluctuations in the vertical velocity (w'), which is calculated as follows:

$$\tau_c = C * w'^2 \tag{A4}$$

where C is a constant, set to 0.9 by Kim et al. (2000).

The bed shear stress due to combined wave-current action (τ_{cw}, N/m^2) was determined using the current-wave model proposed by Grant and Madsen (1979):

$$\tau_{cw} = \sqrt{(\tau_w + \tau_c|\cos\varphi_{cw}|)^2 + (\tau_c|\sin\varphi_{cw}|)^2} \qquad (A5)$$

where τ_w is the bed shear stress due to waves (N/m^2), τ_c is the bed shear stress due to currents (N/m^2), and φ_{cw} is the angle between the current direction and the wave propagation direction (°). The wave propagation direction was estimated by combining the horizontal velocity and pressure data from the ADV measurements using a standard PUV method (http://www.nortekusa.com/usa/knowledge-center/table-of-contents/waves) and MATLAB tools from the Nortek web page that can compute wave directional spectra from Nortek Vector data. These models have been widely used in the estimation of bed shear stress due to current-wave interactions (e.g., Keen and Glenn, 2002; Mellor, 2002; Styles and Glenn, 2002; Feddersen et al., 2003, and references therein).

References

Adam, S., De Backer, A., De Wever, A., Sabbe, K., Toorman, E. A., Vincx, M., Monbaliu, J. (2011). Bio-physical characterization of sediment stability in mudflats using remote sensing: a laboratory experiment. Continental Shelf Research, 31(10), S26-S35.

Andersen, T. J., J. Fredsoe, M. Pejrup (2007), In situ estimation of erosion and deposition thresholds by Acoustic Doppler Velocimeter (ADV), Estuarine Coastal Shelf Sci., 75, 327-336, doi: 10.1016/j.ecss.2007.04.039.

Bale, A. J., J. Widdows, C. B. Harris, J. A. Stephens (2006), Measurements of the critical erosion threshold of surface sediments along the Tamar Estuary using a mini-annular flume, Cont. Shelf Res., 26, 1206-1216

Barbier, E. B. (2013), Valuing Ecosystem Services for Coastal Wetland Protection and Restoration: Progress and Challenges, Resources, 2, 213-230

Boehm, P. D., Quinn, J. G. (1976). The effect of dissolved organic matter in sea water on the uptake of mixed individual hydrocarbons and number 2 fuel oil by a marine filter-feeding bivalve (Mercenaria mercenaria). Estuarine and Coastal Marine Science, 4(1), 93-105.

Bouma, H., Duiker, J. M. C., De Vries, P. P., Herman, P. M. J., Wolff, W. J. (2001). Spatial pattern of early recruitment of Macoma balthica (L.) and Cerastoderma edule (L.) in relation to sediment dynamics on a highly dynamic intertidal sandflat. Journal of Sea Research, 45(2), 79-93.

Burge, C. A., Closek, C. J., Friedman, C. S., Groner, M. L., Jenkins, C. M., Shore-Maggio, A., Welsh, J. E. (2016). The use of filter-feeders to manage disease in a changing world. Integrative and Comparative Biology, 56(4), 573-587.

Carlton, J. T., Thompson, J. K., Schemel, L. E., Nichols, F. H. (1990). Remarkable invasion of San Francisco Bay (California, USA), by the Asian clam Potamocorbula amurensis. I. Introduction and dispersal. Marine Ecology Progress Series, 66, 81-94.

Chen, X., Zong, Y. (1998). Coastal erosion along the Changjiang deltaic shoreline, China: history and prospective. Estuarine, Coastal and Shelf Science, 46(5), 733-742.

Cohen, R. R., Dresler, P. V., Phillips, E. J., Cory, R. L. (1984). The effect of the Asiatic clam, Corbicula fluminea, on phytoplankton of the Potomac River, Maryland. Limnology and Oceanography, 29(1), 170-180.

Collins, M.B., Ke,X., Gao,S., 1998. Tidally-induced flow structure over intertidal flats. Estuarine, Coastal Shelf Sci. 46,233–250.

Dietrich, J.C., Zijlema, M., Westerink, J.J., Holthuijsen, L.H., Dawson, C., Luettich, R.A., Jensen, R.E., Smith, J.M., Stelling, G.S., Stone, G.W., 2011. Modeling hurricane waves and storm surge using integrally-coupled, scalable computations. Coastal Engineering, 58 (1), 45–65.

Dyer, K.R. (2000), Preface (properties of intertidal mudflats), Cont. Shelf Res., 20, 1037-1038pp.

de Brouwer, J. F. C., Bjelic, S., De Deckere, E. M. G. T., Stal, L. J. (2000). Interplay between biology and sedimentology in a mudflat (Biezelingse Ham, Westerschelde, The Netherlands). Continental shelf research, 20(10), 1159-1177.

Eckman, J. E., Nowell, A. R., Jumars, P. A. (1981). Sediment destabilization by animal tubes. Journal of Marine Research, 39(2), 361-373.

Eckman, J. (1983). Hydrodynamic processes affecting benthic recruitment. Limnol. Oceanogr, 28(2), 241-257.

Eisma, D. (1998), Intertidal Deposits: River Mouth, Tidal Flats, and Coastal Lagoons, CRC Press, 459 pp.

Feddersen, F., Gallagher, E. L., Guza, R. T., & Elgar, S. (2003). The drag coefficient, bottom roughness, and wave-breaking in the nearshore. Coastal Engineering, 48(3), 189–195.

Folmer, E. O., Drent, J., Troost, K., Büttger, H., Dankers, N., Jansen, J., Philippart, C. J. (2014).

Large-scale spatial dynamics of intertidal mussel (Mytilus edulis L.) bed coverage in the German and Dutch Wadden Sea. Ecosystems, 17(3), 550-566.

Gage, J. D. (1977). Structure of the abyssal macrobenthic community in the Rockall Trough. In European Symposium on Marine Biology, 11, pp 247-260.

Gao, S. (2009). Geomorphology and sedimentology of tidal flats. In: Perillo, G.M.R., Wolanski, E., Cahoon, D.R., Brinson, M.M. (Eds.), Coastal Wetlands: An Integrated Ecosystem Approach. Elsevier Science, Amsterdam, pp. 295-316.

Gao, S., Du, Y., Xie, W., Gao, W., Wang, D., & Wu, X. (2014). Environment-ecosystem dynamic processes of Spartina alterniflora salt-marshes along the eastern China coastlines. Science China Earth Sciences, 57(11), 2567-2586.

Gerdol, V., Hughes, R. G. (1994). Effect of *Corophium volutator* on the abundance of benthic diatoms, bacteria and sediment stability in two estuaries in southeastern England. Marine Ecology Progress Series, 109-115.

Grabowski, R. C., Droppo, I. G., Wharton, G. 2011. Erodibility of cohesive sediment: the importance of sediment properties. Earth-Science Reviews, 105(3), 101-120.

Grant, W. D., Madsen, O. S. (1979). Combined wave and current interaction with a rough bottom. Journal of Geophysical Research, 84,1797–1808.

Grant, J., Daborn, G. (1994). The effects of bioturbation on sediment transport on an intertidal mudflat. Netherlands Journal of Sea Research, 32(1), 63-72.

Gerwing, T. G., Drolet, D., Hamilton, D. J., & Barbeau, M. A. (2016). Relative importance of biotic and abiotic forces on the composition and dynamics of a soft-sediment intertidal community. PloS one, 11(1), e0147098.

Harris, R. J., Pilditch, C. A., Greenfield, B. L., Moon, V., Kröncke, I. (2016). The Influence of Benthic Macrofauna on the Erodibility of Intertidal Sediments with Varying mud Content in Three New Zealand Estuaries. Estuaries and Coasts, 39(3), 815-828.

Harvey, R. W., & Luoma, S. N. (1985). Effect of adherent bacteria and bacterial extracellular polymers upon assimilation by Macoma balthica of sediment-bound Cd, Zn and Ag. Marine ecology progress series. Oldendorf, 22(3), 281-289.

He, C.B., Xu, S.J., Zhang, C., 1997. Study on the growth and ecological characteristics of Meretrix meretrix cultivated on tidal flat. Chin. J. Fish. Sci. 16, 17 – 20

Jackson, J. L., Webster, D. R., Rahman, S., Weissburg, M. J. (2007). Bed roughness effects on boundary‐layer turbulence and consequences for odor‐tracking behavior of blue crabs (Callinectes sapidus). Limnology and Oceanography, 52(5), 1883-1897.

Keen, T. R., Glenn, S. M. (2002). Predicting bed scour on the continental shelf during hurricane Andrew. Journal of Waterway, Port, Coastal, and Ocean Engineering, 128(6), 249–257.

Kim, S. C., Friedrichs, C. T., Maa, J. P. Y., & Wright, L. D. (2000). Estimating bottom stress in tidal boundary layer from acoustic Doppler velocimeter data. Journal of Hydraulic Engineering, 126(6), 399–406.

Kirby, R. (2000). Practical implications of tidal flat shape. Continental Shelf Research, 20(10), 1061-1077.

Li, L., Jiang, M., Shen, X.J., Wang, Y.L., Yuan, Q., 2014. Culture capacity of Meretrix meretrix in mud flats of Ｒudong，Jiangsu province. Marine environmental science, (5), 752-756.

Li, X. , Bellerby, R. , Craft, C. , Widney, S. E. . (2018). Coastal wetland loss, consequences, and challenges for restoration. Anthropocene Coasts, 1(3), 1-15.

Liu, B., Dong, B., Tang, B., Zhang, T., Xiang, J. 2006. Effect of stocking density on growth, settlement and survival of clam larvae, Meretrix meretrix. Aquaculture, 258(1-4), 344-349.

Luckenbach, M. W. (1986). Sediment stability around animal tubes: The roles of hydrodynamic processes and biotic activity. Limnology and Oceanography, 31(4), 779-787.

McCall, P. (Ed.). (2013). Animal-sediment relations: the biogenic alteration of sediments (Vol.

100). Springer Science & Business Media.

Meadows, P. S., Tait, J. (1989). Modification of sediment permeability and shear strength by two burrowing invertebrates. Marine Biology, 101(1), 75-82.

Meysman, F.J.R., Middelburg, J.J., Heip, C.H.R., 2006. Bioturbation: a fresh look at Darwin's last idea. Trends in Ecology and Evolution 21 (12), 688–695.

Mellor, G. (2002). Oscillatory bottom boundary layers. Journal of Physical Oceanography, 32(11), 3075–3088.

Möller, I., T. Spencer, J.R. French, D.J. Leggett, M. Dixon (2001), The sea-defence value of salt marshes - a review in the light of field evidence from North Norfolk, J. Chartered Institution of Water and Environmental Management, 15, 109-116.

Mouritsen, K. N., Mouritsen, L. T., Jensen, K. T. (1998). Change of topography and sediment characteristics on an intertidal mud-flat following mass-mortality of the amphipod Corophium volutator. Journal of the Marine biological Association of the United Kingdom, 78(4), 1167-1180.

Mouritsen, K. N., Poulin, R. (2002). Parasitism, community structure and biodiversity in intertidal ecosystems. Parasitology, 124(07), 101-117.

Na, H., 2004. Jiangsu Rudong clam industry faces problems. Modern fisheries information, 19(5), 31-31.

Navarro, E., Iglesias, J. I. P., Camacho, A. P., Labarta, U., Beiras, R. 1991. The physiological energetics of mussels (*Mytilus galloprovincialis Lmk*) from different cultivation rafts in the Ria de Arosa (Galicia, NW Spain). Aquaculture, 94(2-3), 197-212.

Navarro, J. M., González, K., Cisternas, B., López, J. A., Chaparro, O. R., Segura, C. J., Labarta, U. (2014). Contrasting physiological responses of two populations of the razor clam Tagelus dombeii with different histories of exposure to paralytic shellfish poisoning (PSP). PloS one, 9(8), e105794.

Nasermoaddeli, M. H., Kösters, F., Hofmeister, R., Lemmen, C., & Wirtz, K. W. (2014). First results of modelling benthos influence on sediment entrainment using a generic approach within the MOSSCO framework. In 11 International Conference on Hydroscience and Engineering (ICHE), Hamburg, Germany (Vol. 28).

Nehls, G., Tiedemann, R. (1993). What determines the densities of feeding birds on tidal flats? A case study on Dunlin, Calidris alpina, in the Wadden Sea. Netherlands Journal of Sea Research, 31(4), 375-384.

Needham, H. R., Pilditch, C. A., Lohrer, A. M., Thrush, S. F. (2013). Density and habitat dependent effects of *crab* burrows on sediment erodibility. Journal of sea research, 76, 94-104.

Nowell, A. R., Jumars, P. A., Eckman, J. E. (1981). Effects of biological activity on the entrainment of marine sediments. Marine Geology, 42(1-4), 133-153.

O'riordan, C. A., Monismith, S. G., Koseff, J. R. (1995). The effect of bivalve excurrent jet dynamics on mass transfer in a benthic boundary layer. Limnology and Oceanography, 40(2), 330-344.

Orvain, F., Sauriau, P. G., Sygut, A., Joassard, L., & Le Hir, P. (2004). Interacting effects of Hydrobia ulvae bioturbation and microphytobenthos on the erodibility of mudflat sediments. Marine ecology progress series, 278, 205-223.

Paterson, D. M., Black, K. S. (1999). Water flow, sediment dynamics and benthic biology. Advances in Ecological Research, 29(155-193).

Resio, D. T. , Westerink, J.J. 2008. Modeling the physics of storm surges. Physics Today, 61(9), 33-38.

Rhoads, D. C., Boyer, L. F. (1982). The effects of marine benthos on physical properties of sediments. In Animal-sediment relations (pp. 3-52). Springer US.

Salehi, M., K. Strom (2012), Measurement of critical shear stress of mud mixtures in the San

Jacinto estuary under different wave and current combinations, Cont. Shelf Res., 47, 78-92

Scoffin, T. P. (1970). The trapping and binding of subtidal carbonate sediments by marine vegetation in Bimini Lagoon, Bahamas. Journal of Sedimentary Research, 40(1).

Shen, B. 2004. The problems and Countermeasures of clam industry in Jiangsu County of Rudong province development status. Fishing Guide, 1, 46-47 (In Chinese).

Shi, B.W., Y.P. Wang, Y.Yang, M.L.Li, P. Li, W.F. Ni, J.H. Gao. 2015. Determination of critical shear stresses for erosion and deposition based on in situ measurements of currents and waves over an intertidal mudflat, J. Coastal Res, 31, 1344-1356.

Styles, R., & Glenn, S. M. (2002). Modeling bottom roughness in the presence of wave-generated ripples. Journal of Geophysical Research, 107(C8), 3110. https://doi.org/10.1029/200 1JC000864

Tallqvist, M. (2001). Burrowing behaviour of the Baltic clam Macoma balthica: effects of sediment type, hypoxia and predator presence. Marine Ecology Progress Series, 212, 183-191.

Tolhurst, T. J., Riethmüller, R., & Paterson, D. M. (2000). In situ versus laboratory analysis of sediment stability from intertidal mudflats. Continental Shelf Research, 20(10), 1317-1334.

Venier, C., da Silva, J. F., McLelland, S. J., Duck, R. W., & Lanzoni, S. (2012). Experimental investigation of the impact of macroalgal mats on flow dynamics and sediment stability in shallow tidal areas. Estuarine, Coastal and Shelf Science, 112, 52-60.

Wang Y., Zhu D.K. 1994. Tidal flats in china. In: Zhou, Di., Liang, Y.B., Tseng, C.K. (Eds.), Oceanology of China seas. Springer Science and Business Media, pp. 445-456.

Wang, Y. P., Gao, S., Jia, J., Thompson, C. E., Gao, J., Yang, Y. (2012). Sediment transport over an accretional intertidal flat with influences of reclamation, Jiangsu coast, China. Marine Geology, 291, 147-161.

Ward, J.E., and Shumway, S.E. 2004 . Separating the grain from the chaff: particle selection in suspension -and deposit - feeding bivalves. Journal of Experimental Marine Biology and Ecology, 300, 83–130 .

Willows, R. I., Widdows, J., --Wood, R. G. 1998. Influence of an infaunal bivalve on the erosion of an intertidal cohesive sediment: a flume and modeling study. Limnology and Oceanography, 43(6), 1332-1343.

Widdows, J., Brinsley, M. D., Bowley, N., Barrett, C. 1998a. A benthic annular flume forin situmeasurement of suspension feeding/biodeposition rates and erosion potential of intertidal cohesive sediments. Estuarine, Coastal and Shelf Science, 46(1), 27-38.

Widdows, J., Brinsley, M. D., Salkeld, P. N., Elliott, M. 1998b. Use of annular flumes to determine the influence of current velocity and bivalves on material flux at the sediment-water interface. Estuaries, 21(4), 552-559.

Widdows, J., Brinsley, M. D., Salkeld, P. N., Lucas, C. H. 2000. Influence of biota on spatial and temporal variation in sediment erodability and material flux on a tidal flat (Westerschelde, The Netherlands). Marine Ecology Progress Series, 194, 23-37.

Widdows, J., Lucas, J. S., Brinsley, M. D., Salkeld, P. N., Staff, F. J. 2002. Investigation of the effects of current velocity on mussel feeding and mussel bed stability using an annular flume. Helgoland Marine Research, 56(1), 3–12.

Widdows, J., Brinsley, M. 2002. Impact of biotic and abiotic processes on sediment dynamics and the consequences to the structure and functioning of the intertidal zone. Journal of Sea Research, 48(2), 143-156.

Wood, P. J., Armitage, P. D. (1997). Biological effects of fine sediment in the lotic environment. Environmental management, 21(2), 203-217.

Wotton, R. S., Malmqvist, B. (2001). Feces in aquatic ecosystems. BioScience, 51(7), 537-544.

Wu, G.X., Li, H. , Liang, B. , Shi, F. , Kirby, J. T. , Mieras, R. 2017. Subgrid modeling of salt marsh hydrodynamics with effects of vegetation and vegetation zonation. Earth Surface Processes and Landforms, 42, 1755–1768.

Wu, G.X., Shi, F.Y., Kirby, J.T., Liang, B.C., Shi, J. 2018. Modeling wave effects on storm surge and coastal inundation, Coastal Engineering, 140: 371-382.

Xing, F., Y. P. Wang, H. V. Wang (2012), Tidal hydrodynamics and fine-grained sediment transport on the radial sand ridge system in the southern Yellow Sea, Mar. Geol., 291, 192-210.

Yu, Q., Niu, M., Yu, M., Liu, Y., Wang, D., Shi, X. (2016). Prevalence and antimicrobial susceptibility of Vibrio parahaemolyticus isolated from retail shellfish in Shanghai. Food Control, 60, 263-268.

Zhao, Y.Y., Gao, S., 2015. Simulation of Tidal Flat Sedimentation in Response to Typhoon—induced Storm Surges：A case study from Rudong Coast，Jiangsu，China. ACTA SEDIMENTOLOGICA SINICA, 33(1): 79-90 (In Chinese).

Zhuang, S. H., Wang, Z. Q. (2004). Influence of size, habitat and food concentration on the feeding ecology of the bivalve, Meretrix meretrix Linnaeus. Aquaculture, 241(1), 689-699.
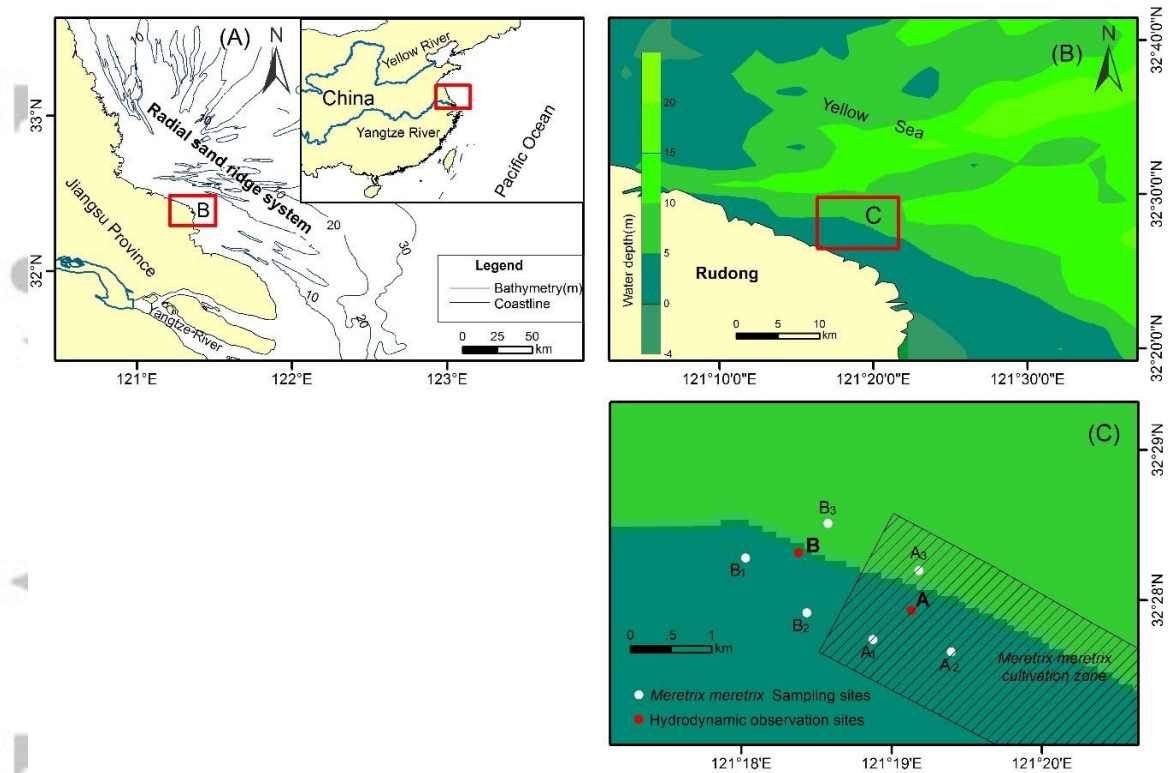
Fig. 1 Location of the study area (A), bathymetry of the Rudong intertidal flat (B), and sites of *in situ Meretrix meretrix* (*M. meretrix*) sampling and hydrodynamic observations (C). In Fig 1. C, white circles denote *M. meretrix* sampling sites (A_1-A_3 and B_1-B_3), and red circles denote hydrodynamic observation sites (A and B). The shaded rectangle is the cultivation zone with *Meretrix meretrix*.
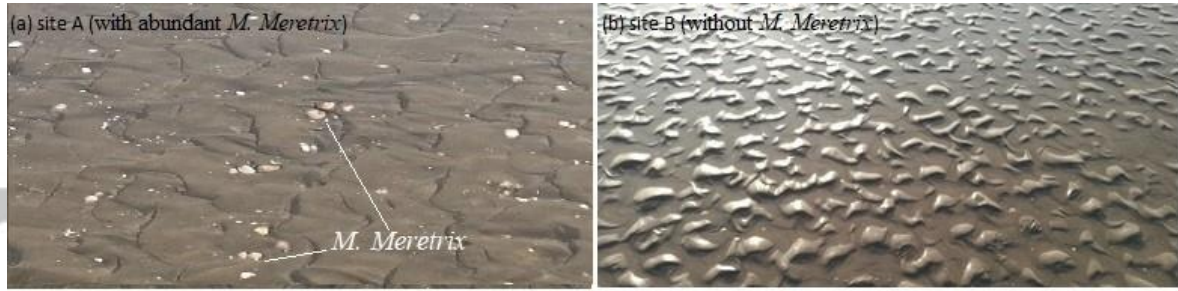
Fig. 2 Photographs of (a) site A, with abundant *M. meretrix*, and (b) site B, without *M. meretrix*.
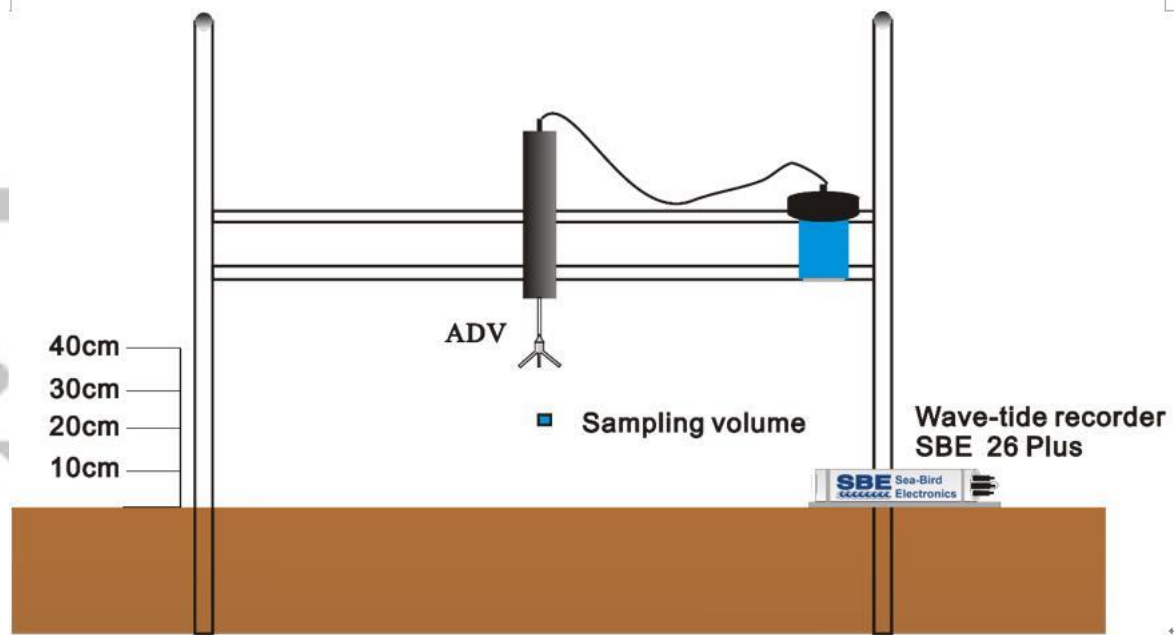
Fig. 3 Schematic diagram of the hydrodynamic observation equipment showing heights of the ADV sensors for measurements of turbulent flow velocity and bed-level change and the pressure sensors of the wave-tide recorder (SBE 26 Plus) for wave measurements. The blue square denotes the ADV sampling volume, which is a cylinder (14.9 mm in length and 15 mm in diameter) when the ADV instrument measures three-dimensional velocity. The pressure sensor of wave-tide recorder SBE 26 Plus is located at a height of 10 cm above the sea bed.
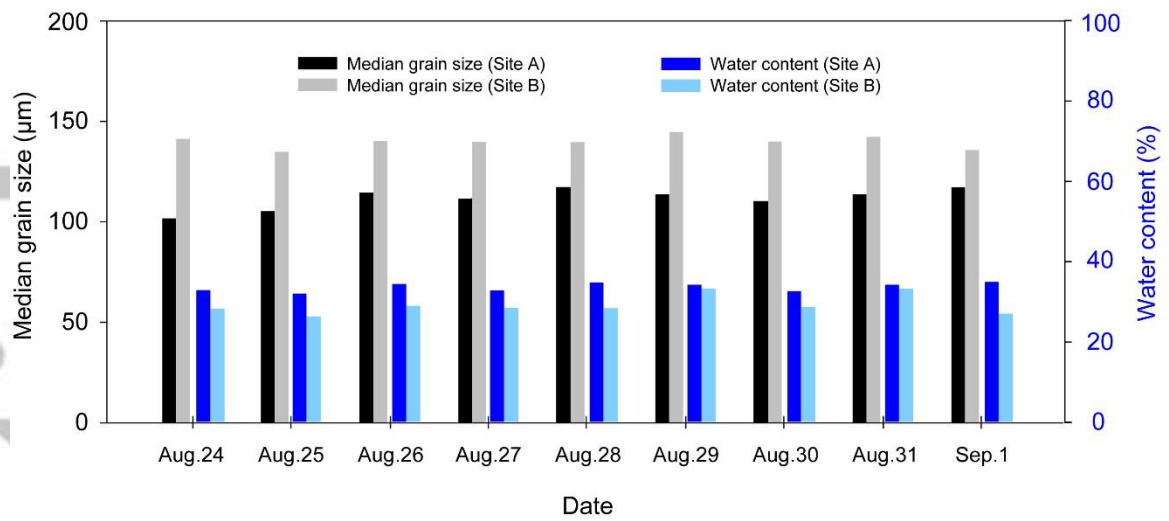
Fig. 4 Daily median grain size and water content at site A (with abundant *M. meretrix*) and site B (without *M. meretrix*) during the data collection period (24 August to 1 September 2016).
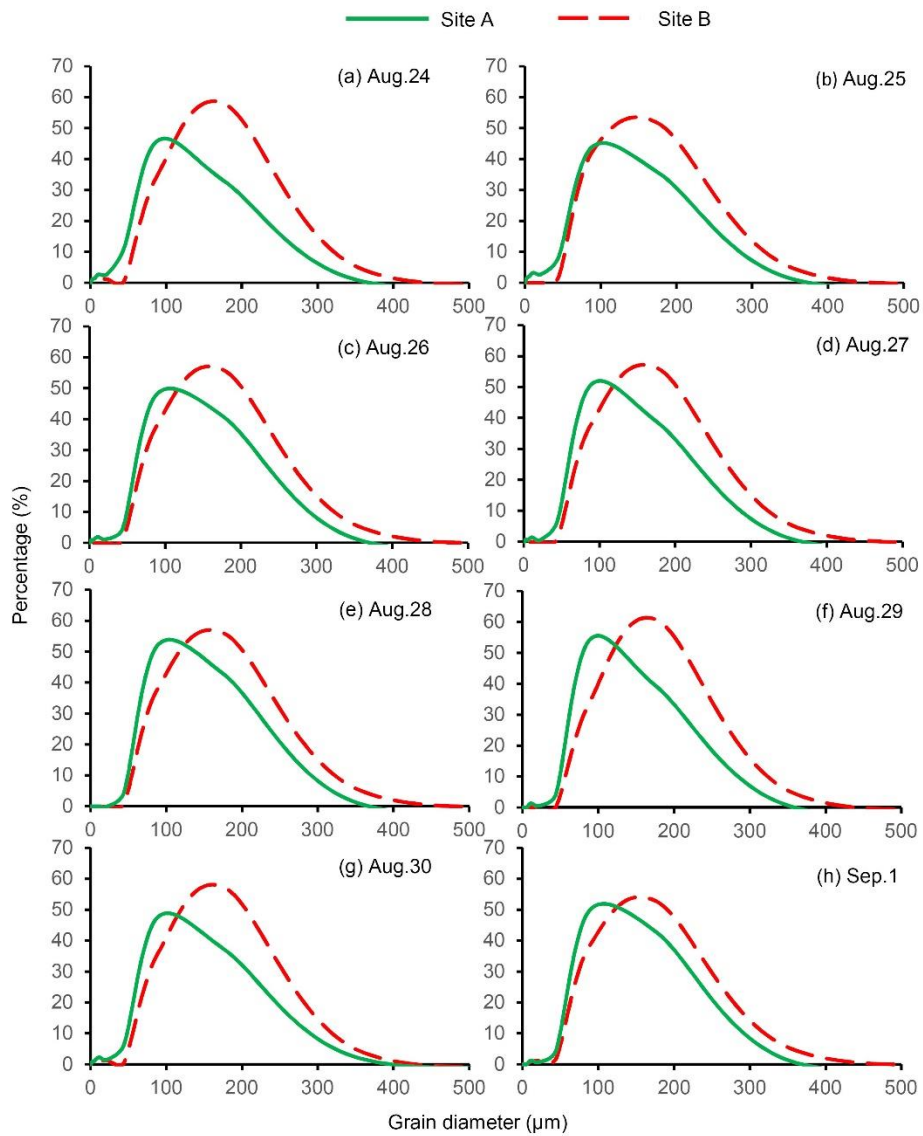
Fig. 5 Grain-size distribution of bottom sediment at site A (with abundant *M. meretrix*) and B (without *M. meretrix*) during field measurement.
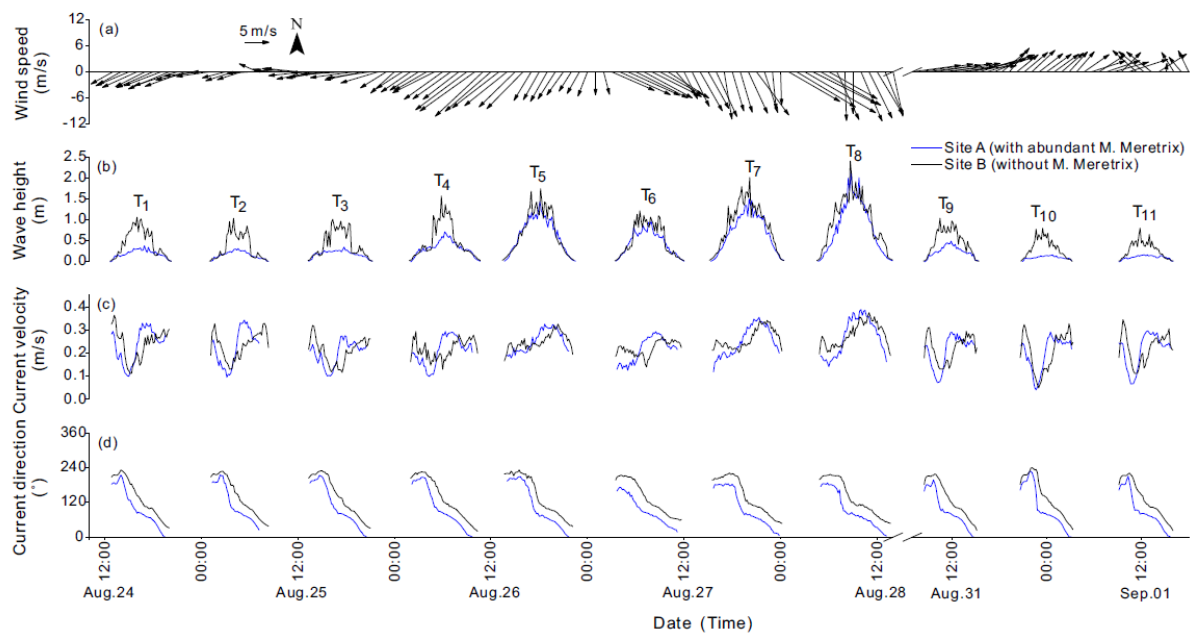
Fig. 6 Time series of (a) wind, (b) wave height, (c) current velocity, and (d) current direction at site A (with abundant *M. meretrix*) and B (without *M. meretrix*). Note: the time (date) in the panel is local Beijing time.
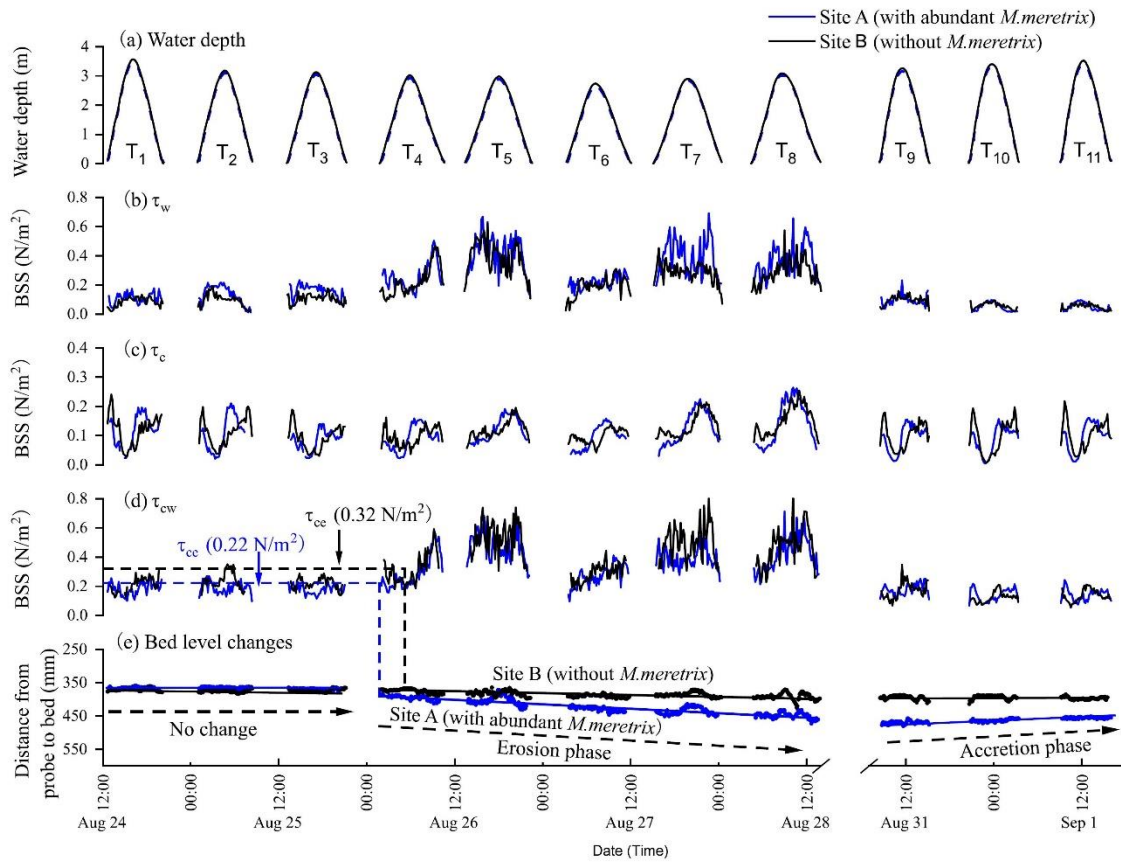
Fig. 7 Time series data of water depth (a); bed shear stress due to waves (τ_w, b), currents (τ_c, c), and combined wave-current action (τ_{cw}, d); and bed elevation (e). Dotted lines in (d) and (e) indicate the estimated critical shear stress for the erosion of bottom sediment (τ_{ce}), which was 0.22 N/m^2 for site A and 0.32 N/m^2 for site B.
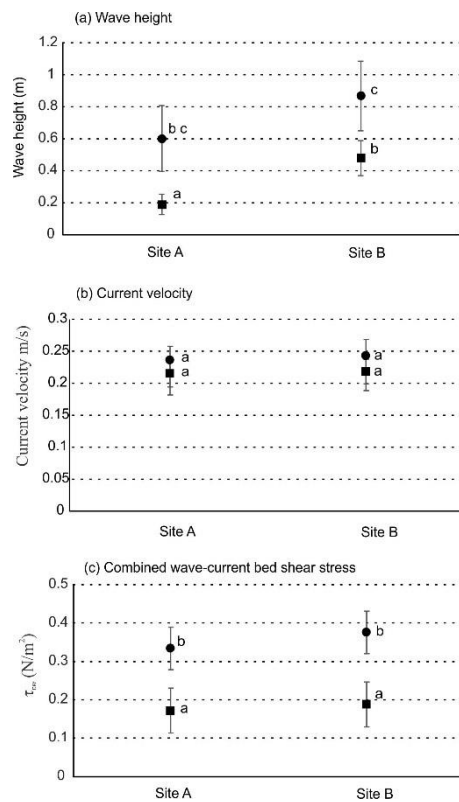
Fig. 8 Mean and standard deviation values by site and wind regime for a) wave height, b) current velocity, and c) combined wave and current bed shear stress (τ_{cw}). Squares represent tides grouped under wind Regime I and circles represent tides under wind Regime II. Different letters denote significant differences ($p<0.01$) between treatments.

Table 1 Instrument settings and parameters used for hydrodynamic measurements.

Instruments	Height above seabed	Measured accuracy	Sampling frequency	Measured physical parameters	Interval	Sampling numbers per burst
ADV	37 cm	±1 mm (vertical distance)	16 Hz	Turbulent velocity and bed elevation	5 min	4096
Wave-tide recorder SBE 26 Plus	10 cm	0.01% of full scale	4 Hz	Water depth, wave height and wave period	10 min	1024

Table 2 Quantity, density, and average dimensions of *M. meretrix* in sediment samples from sites A and B.

Sites		Sampling condition			Size of *M. meretrix*			
		Number	Area (m^2)	Density (indiv./m^2)	Length (mm)	Width (mm)	Height (mm)	Weight (g)
A	A_1	11	0.09	122	30.5±4.0	25.5±3.3	15.1±2.3	7.8±3.1
	A_2	15	0.09	167	30.8±4.9	24.8±3.3	15.6±2.6	8.5±4.7
	A_3	11	0.09	122	31.7±5.6	26.9±4.6	15.9±2.8	8.9±5.4
B	B_1	0	0.09	0	0.0±0.0	0.0±0.0	0.0±0.0	0.0±0.0
	B_2	0	0.09	0	0.0±0.0	0.0±0.0	0.0±0.0	0.0±0.0
	B_3	1	0.09	11	40.3±0.0	34.1±0.0	20.6±0.0	17.8±0.0

Indiv./m^2 denotes the number of *M. meretrix* individuals per m^2

Table 3 Comparison of hydrodynamic (tidal-averaged τ_w, τ_c, and τ_{cw}) and bed-level changes between sites A (with abundant *M. meretrix*) and B (without *M. meretrix*).

| Tides | Tidal-averaged τ_w (N/m^2) | | Tidal-averaged τ_c (N/m^2) | | Tidal-averaged τ_{cw} (N/m^2) | | Bed-level changes (mm) | | | |
| | Site A | Site B | Site A | Site B | Site A | Site B | Site A | Site B | Erosion/accretion phase | |
									Site A	Site B
T_1	0.109±0.036	0.086±0.032	0.119±0.055	0.106±0.040	0.097±0.066	0.110±0.071	-0.990	-0.620	No change (T_1-T_3)	No change (T_1-T_3)
T_2	0.135±0.064	0.096±0.043	0.106±0.063	0.105±0.046	0.116±0.076	0.158±0.086	-0.870	+0.390		
T_3	0.161±0.040	0.105±0.032	0.083±0.036	0.082±0.034	0.106±0.074	0.133±0.106	+0.633	+1.167		
T_4	0.253±0.090	0.222±0.102	0.091±0.029	0.090±0.046	0.231±0.075	0.242±0.083	-19.570	-13.3	-97 (T_4-T_8) (erosion phase)	-39 (T_4-T_8) (erosion phase)
T_5	0.411±0.129	0.384±0.115	0.129±0.028	0.125±0.042	0.361±0.170	0.382±0.174	-19.300	-15.800		
T_6	0.222±0.043	0.189±0.067	0.098±0.025	0.094±0.042	0.170±0.086	0.175±0.094	-13.69	-0.600		
T_7	0.389±0.127	0.286±0.067	0.138±0.043	0.132±0.056	0.274±0.148	0.371±0.182	-9.640	-6.900		
T_8	0.359±0.112	0.285±0.086	0.158±0.050	0.150±0.074	0.228±0.156	0.269±0.131	-13.45	-3.600		
T_9	0.096±0.023	0.095±0.037	0.092±0.040	0.090±0.048	0.088±0.063	0.098±0.064	+5.790	+1.050	+30 (T_9-T_{11}) (accretion phase)	+15 (T_9-T_{11}) (accretion phase)
T_{10}	0.057±0.021	0.048±0.029	0.085±0.056	0.083±0.046	0.080±0.044	0.093±0.046	+7.420	+5.510		
T_{11}	0.050±0.027	0.049±0.019	0.095±0.052	0.093±0.041	0.094±0.041	0.107±0.040	+2.370	+1.630		

"/" indicates no data;
"-" indicates erosion, and "+" indicates accretion.